Preliminary Experiments on a CRLH Metamaterial Zeroth-Order Resonant Coil (ZORC) Element for 7 Tesla MRI Applications with Large Field of View

A. Rennings[1], **P. Schneider**[1], **C. Caloz**[2], **S. Orzada**[3]

[1] General and Theoretical Electrical Engineering (ATE), University of Duisburg-Essen, 47048 Duisburg, Germany; Fax: +49 203 379-3499; Email: andre.rennings@uni-due.de

[2] Poly-Grames Research Center, École Polytechnique de Montréal, Montréal, H3T 1J4, Québec, Canada; Fax: +1 514 340-5892; Email: christophe.caloz@polymtl.ca

[3] Erwin L. Hahn Institute for MRI, University of Duisburg-Essen, 45141 Essen, Germany

Abstract

Preliminary experimental magnetic resonance imaging (MRI) results based on a novel composite right/left-handed (CRLH) zeroth-order resonant coil (ZORC) are presented. These results demonstrate, using an homogeneous flat phantom emulating the human body, that the ZORC can achieve very large fields of view, corresponding to the length of the ZOR structure, which is of approximately 30 cm in the prototype presented.

1. Introduction

A novel composite right/left-handed (CRLH) [1] zeroth-order resonant coil (ZORC) providing large fields of view in magnetic resonance imaging (MRI) [2] was theoretically introduced in [3]. This ZORC exploits the unique RF field uniformity of CRLH resonant antennas operated at the transition frequency between the left-handed and right-handed bands [1], where the guided wavelength is infinite ($\lambda_g = 2\pi/\beta \to \infty$). This ZORC is particularly suited to sagittal and coronal MRI sections, where a long field of view enables faster MRI processing, by suppressing the necessity to move the body. This paper presents preliminary experimental results of ZORC MRI and compares them with near-field FDTD predictions, using an homogeneous flat phantom emulating the human body.

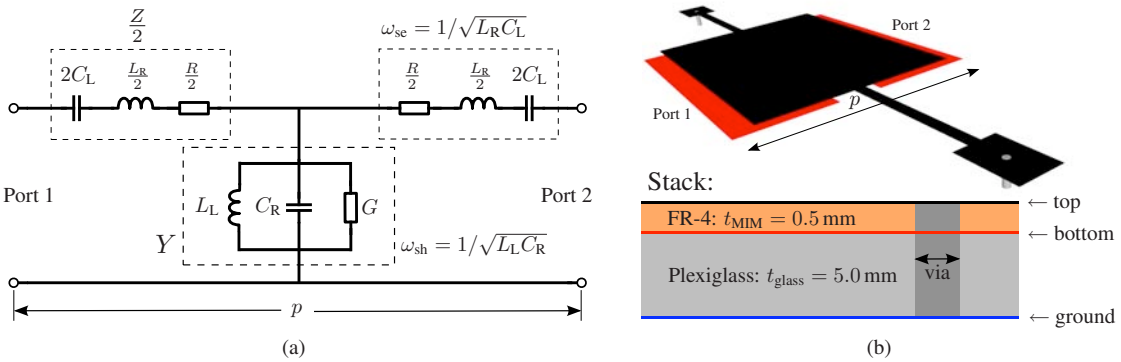

Fig. 1: Unit cell of the periodic metal-insulator-metal (MIM) ZORC element. (a) Lossy equivalent circuit in T-topology for the symmetric (with respect to the stubs) CRLH unit cell. (b) Perspective view and multilayer profile with top/bottom metal layer for upper/lower MIM plates and ground plane ($\varepsilon_{FR4} = 4.7$, $\varepsilon_{plexiglass} = 2.2$, $p = 60.5$ mm, line width of 75 mm, stub length of 45.5 mm, stub width of 3 mm, via holes of diameter 1.5 mm).

ISBN 978-0-9551179-6-1

2. ZORC Element with Longitudinally Uniform Fields

Although the complete ZORC incorporates several ZORC elements combined together so as to build a cylinder with a polygonal cross section around the body to image, we will consider here only one of these elements. This will provide preliminary characterization of the magnetic field longitudinal uniformity. Fig. 1 shows the circuit model and layout of the CRLH ZORC element unit cell, while Fig. 2 shows the complete 5-cell ZORC element considered in this paper along with the uniform magnetic field distribution achieved above the structure. The extracted CRLH parameters are $C_{\mathrm{L}} = 19.2\,\mathrm{pF}$, $C_{\mathrm{R}} = 6.4\,\mathrm{pF}$, $L_{\mathrm{L}} = 42.9\,\mathrm{nH}$, $L_{\mathrm{R}} = 14.6\,\mathrm{nH}$, $R = 650\,\mathrm{m\Omega}$, $G = 64.4\,\mu\mathrm{S}$, resulting in the resonance frequencies $f_{\mathrm{se}} = 305\,\mathrm{MHz}$ and $f_{\mathrm{sh}} = 308\,\mathrm{MHz}$, and the Q-factors $Q_{\mathrm{se}} = 42$ and $Q_{\mathrm{sh}} = 190$. The ZORC is designed to operate in its series mode, i.e. at the frequency $\omega_{\mathrm{se}} = 1/\sqrt{L_{\mathrm{R}}C_{\mathrm{L}}}$, where the structure is terminated by a short [4]. In this mode, the energy is mainly concentrated in the series elements, i.e. along the axis of the structure. Two anti-parallel stubs are placed in each unit cell in order to minimize unwanted longitudinal magnetic field components caused by the transverse currents. The electric and magnetic fields are polarized along and perpendicularly to the axis of the structure, respectively. Since the ZORC element will be placed together with other ZORC elements to build a cylindrical MRI structure along the axis of the DC magnetic field, this polarization configuration satisfies the requirement for generating an RF field perpendicular to the MRI DC field.

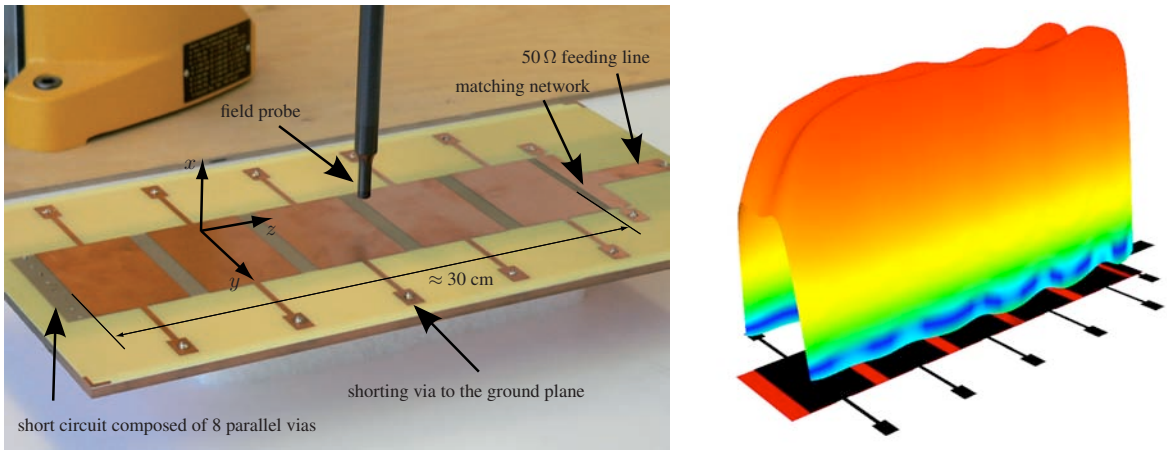

(a) (b)

Fig. 2: Prototype (a) and FDTD-simulated longitudinally uniform magnetic field component H_y 2 cm above the ZORC structure (b).

3. Results

Fig. 3 displays the FDTD-simulated and measured near-fields on top of the ZORC element in the setup of Fig. 4(a) with and without the phantom load, respectively. Excellent longitudinal near-field uniformity is observed in both the unloaded and loaded cases. Such a feature is a requirement for high-quality MRI, since the entire body is completely immersed in the near-field of the energy produced in the MRI tube. Interestingly, the flux enhancement due to the load tends to uniformize the transverse field distribution, which exhibits a valley in the unloaded case due to the crowding-out effect of the electric current density to the edges of the strips. Fig. 4(b) shows two B_1-maps representing the so-called *flip angle* [2] of the corresponding voxel in the flat phantom and indicates the maximal possible field of view (smooth zones). Preliminary MRI pictures are shown in Fig. 5, where the flat phantom is clearly identified in the sagittal plane. The top part (liquid surface) is less visible, due to field attenuation, but this may be corrected by adding a ZORC element to the other side.

Acknowledgment

The authors wish to thank A. Rahn for carrying out the near-field measurements at IMST GmbH in Kamp-Lintfort, Germany and the University of Duisburg-Essen for financial support of our MRI activity (“Programm zur Förderung des promovierten wissenschaftlichen Nachwuchses”).

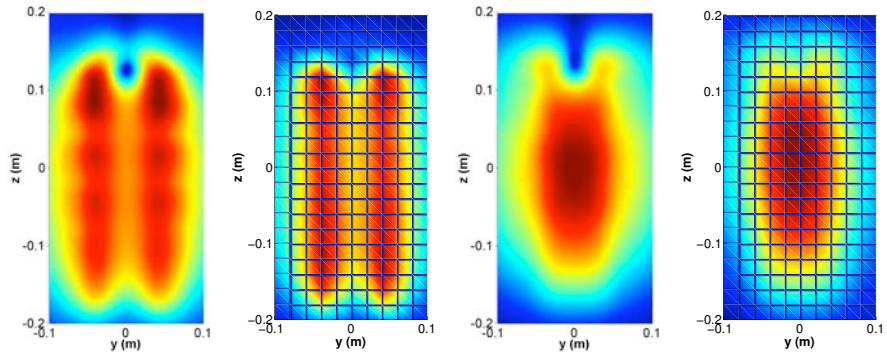

(a) $|\boldsymbol{H}_{\text{unloaded}}|$ FDTD (b) $|\boldsymbol{H}_{\text{unloaded}}|$ Meas. (c) $|\boldsymbol{H}_{\text{loaded}}|$ FDTD (d) $|\boldsymbol{H}_{\text{loaded}}|$ Meas.

Fig. 3: Magnetic field amplitude distribution (FDTD vs. measurement) 25 mm above the ZORC element for the unloaded and loaded cases. For the later the configuration depicted in Fig. 4(a) is used.

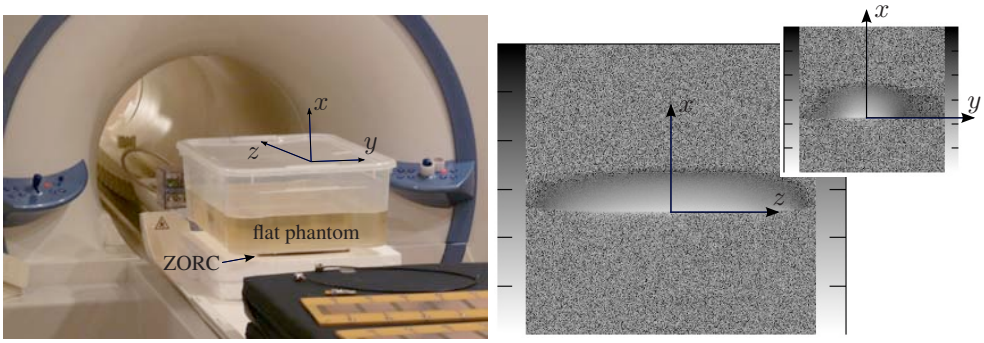

(a) (b)

Fig. 4: CRLH ZORC element testing below a body-emulating flat phantom ($\varepsilon_{\text{r}} = 46$ and $\sigma = 0.86\,\text{S/m}$) in front of the 7-Tesla MRI tomograph (a) and B_1-sensitivity-maps of the element indicating the possible field of view (b).

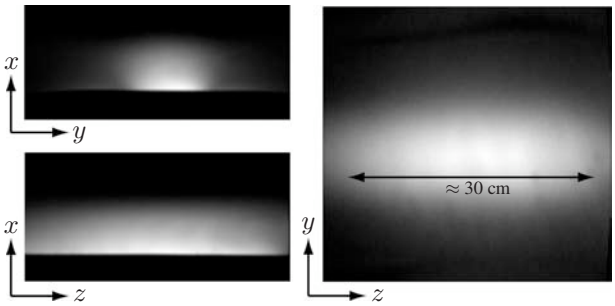

Fig. 5: MRI of the flat phantom setup of Fig. 4(a) for sagittal (xz), transversal (xy) and coronal (yz) cuts.

References

[1] C. Caloz and T. Itoh, *Electromagnetic Metamaterials, Transmission Line Theory and Microwave Applications.* Wiley and IEEE Press, 2005.

[2] R. H. Hashemi, W. G. Bradely, and C. J. Lisanti, *MRI - The Basics,* Lippincott Williams & Wilkins, 2004.

[3] A. Rennings, J. Mosig, A. Bahr, C. Caloz, M. E. Ladd, and D. Erni, "A CRLH metamaterial based RF coil element for magnetic resonance imaging at 7 Tesla," in Proc. *3rd European Conference on Antennas and Propagation (EuCAP)*, Berlin, Germany, pp. 3231-3234, March 2009.

[4] A. Rennings, T. Liebig, C. Caloz, and P. Waldow, "MIM CRLH series-mode zeroth-order resonant antenna (ZORA) implemented in LTCC technology," in Proc. *APMC*, Bankok, Thailand, pp. 191-194, Dec. 2007.

